Entrepreneurship Journal for Finance and Business (EJFB)
2026, VOL. 07, NO. special, 314-322, E-ISSN: 2709-4251, P-ISSN: 2708-8790
DOI: https://doi.org/10.56967/ejfb2026940

Compositionally engineered TiO_2–SiO_2 mixed dielectric thin films as a single-layer broadband beam splitter: Design, fabrication, and optical performance

Lana F. Sahal [1], Husamuldeen Q. Mousa [2], Ghufran A. Sabah [3*]
[1] Department of Postgraduate Studies, College of Medicine, University of Baghdad, Baghdad, Iraq
[2] Ministry of Education, Babil Education Directorate, Hilla Preparatory School for Boys, Hilla, Iraq
[3] Department of Medical Instrumentation Techniques, Polytechnic College of Engineering Specializations-Baghdad, Middle Technical University, Baghdad, Iraq
lana.farook1204a@csw.uobaghdad.edu.iq , husamaldeen498@gmail.com , ghufran.ahmed@mtu.edu.iq

Article information:
Published: 25–05– 2026

***Corresponding author:**
Ghufran A. Sabah
ghufran.ahmed@mtu.edu.iq

This work is licensed under a Creative Commons Attribution 4.0 International License.

Abstract:

Standard multilayer dielectric beam splitter is limited by spectrum interference ripples, high production complexity and strict tolerance of the thickness. Here we report a compositionally tuned TiO2-SiO2 mixed dielectric thin film as an effective single-layer broadband beam splitter. The composite films were produced on glass substrates with pulsed laser deposition (PLD) which allowed fine control over layer thickness and equilibrium stoichiometry by varying the number of laser pulses. The TiO_2:SiO_2 ratio was optimized using the effective medium model of Lorentz-Lorenz to attain a refractive index in between (~1.95-2.05) for controlled amplitude division with no multilayer interference stacking. X-ray diffraction (XRD) study revealed a nanostructured mixed-phase morphology using crystallite sizes in the range of 16-46 nm, ideal for low-scattering optical applications. The transmission-reflection ratios were steady and adjustable from 65/35 to 80/20 with small spectral ripples ($\Delta T_ripple < 4\%$) as demonstrated by UV–Vis–NIR spectroscopy in the range 400–1100 nm. The experimental results agree well with transfer matrix method (TMM) simulations, which validates the effective refractive index technique. The suggested single-layer design outperforms existing multilayer designs in terms of structural complexity, thickness sensitivity and number of manufacturing processes, while maintaining broadband and spectrally flat optical performance. Here, we show a simple and scalable way to achieve broadband beam splitting by changing the refractive index in a single dielectric layer.

Keywords: TiO_2–SiO_2 composite, Single-layer beam splitter, Dielectric thin films, Pulsed laser deposition, Effective medium theory,Transfer matrix technique.

1.Introduction

Optical beam splitters are crucial components of many modern photonic and optoelectronic systems, for example, laser interferometers, optical communication systems, imaging systems and photovoltaic devices [1]. Their main function is to split an incident optical beam through reflected and transmitted parts with a specified intensity ratio throughout a given spectral range. However, it is still difficult to realize broadband and spectrally uniform beam splitting, especially in the presence of requirements for compactness, simplicity of manufacture and optical stability [2]. Typical dielectric beam splitters employ interference coatings consisting of alternating high and low refractive index materials in

Entrepreneurship Journal for Finance and Business (EJFB)
2026, VOL. 07, NO. special, 314-322, E-ISSN: 2709-4251, P-ISSN: 2708-8790
DOI: https://doi.org/10.56967/ejfb2026940

multilayer stacks [3]. These multilayer stacks give design freedom but typically require 10–30 layers with total thickness in the micrometer range. This structural intricacy gives rise to numerous disadvantages: long deposition durations, cumulative mistakes in thickness, significant susceptibility to imperfections in the deposition and conspicuous spectral ripples owing to high-order Fabry–Pérot interference [4]. These restrictions have driven the quest for alternate beam-splitting techniques that minimize structural complexity while preserving broadband performance. Single-layer beam splitters are an interesting option because of their simplicity and lower sensitivity to thickness. However, most of the reported single-layer designs are based on fixed index materials, nanostructured metasurfaces or lithographically patterned structures [5]. Such designs often suffer from restricted bandwidth, large spectrum fluctuations or complex fabrication requirements [6]. Gradient index films and metamaterial-based techniques have been investigated but often need intricate deposition control or nanoscale patterning, which hinders scalability and cost effectiveness [7,19]. Another approach is to use refractive index engineering with dielectric mixing [8]. By mixing two dielectric materials with greatly differing refractive indices, the effective refractive index of a single layer may be adjusted constantly. This method allows regulated splitting of the amplitude with little change in spectrum. The Lorentz–Lorenz model and associated effective medium theories offer a sound theoretical foundation for the prediction of the optical response of these mixed dielectric systems [9]. TiO_2 and SiO_2 are good choices for this purpose, since they have wide ranges of optical transparency, significant refractive index contrasts and chemical stability. TiO_2 has a high refractive index ($n \approx 2.6$) in the visible to near-infrared region. SiO_2 is a low-index ($n \approx 1.46$), low-loss dielectric matrix. TiO_2 and SiO_2 composite films show intermediate and tunable refractive indices, which are suited for broadband beam-splitting applications by mixing appropriate quantities. Pulsed laser deposition (PLD) allows an excellent control over composition, thickness and microstructure in a single deposition step and hence is of great benefit for compositional engineering [10,18].

The work presents a novel composition-engineered single-layer TiO_2 -SiO_2 mixed dielectric thin film, synthesized via PLD, designed as a broadband beam splitter (400–1100 nm) with moderate ripple interference (<4%). This film allows for tunable amplitude division (65/35 to 80/20) by adjusting the effective refractive index (1.95–2.05) in a sub-micrometer layer (<500 nm), offering a simpler alternative to complex multilayer stacks. Utilization of Lorentz–Lorenz theory and Transfer Matrix Method (TMM) with room-temperature PLD optimization enhances scalability and reduces scattering compared to traditional lithographic metasurfaces and coatings. Although the Lorentz–Lorenz model and TMM are standard theoretical frameworks widely utilized in thin-film optics, their application in guiding single-step pulsed laser deposition to bypass multilayer complexities remains insufficiently explored in recent literature

2. Materials and Methods

2.1. Film Deposition via Pulsed Laser Deposition

The TiO_2–SiO_2 composite dielectric thin films were grown on the well-polished glass substrates by pulsed laser deposition (PLD) technique using a KrF excimer laser at a wavelength λ of 248nm. The deposition chamber was first evacuated to a base pressure of ($1.0 * 10^{-5}$ mbar) before adding oxygen as reactive gas to maintain a working chamber pressure of($2.5 *10^{-2}$ mbar) throughout growth. The target material was ablated by a laser pulse with energy 800mJ, pulse duration 20ns and repetition rate 5Hz as shown in table 1. The composite target was continually rotated to guarantee optimum uniformity of the composition and to avoid local deterioration. The distance between the target and the substrate was regulated to 50 mm. The average deposition rate was calculated to be around 1.93nm/pulse under these adjusted laser and geometric parameters, which allows exact control of film thickness by the total number of laser pulses (75, 175 and 200 pulses).

Entrepreneurship Journal for Finance and Business (EJFB)
2026, VOL. 07, NO. special, 314-322, E-ISSN: 2709-4251, P-ISSN: 2708-8790
DOI: https://doi.org/10.56967/ejfb2026940

Table 1: **Optimized Pulsed Laser Deposition (PLD) operational parameters for TiO_2–SiO_2 thin films.**

Operational Value / Specification	PLD Process Parameter
KrF Excimer Laser 248 nm	**Laser Source / Wavelength**
20 ns	**Pulse Duration**
800 mJ	**Laser Pulse Energy**
5 Hz	**Repetition Rate**
2.5 *10-2mbar	**Working Chamber Pressure**
50 mm	**Target-to-Substrate Distance**
~ 1.93nm/pulse	**Calibrated Deposition Rate**
75, 175, 200 pulses	**Total Pulse Variation**

2.2. Structural Characterization

The structural characteristics of the deposited films were studied by X-ray diffraction (XRD) using Cu Kα radiation (λ = 1.5406 Å). Diffraction patterns were recorded in step scan mode from 10° to 80° in 2θ. The phase identification was conducted by comparison with the standard JCPDS reference cards. The mean crystallite size was calculated from particularly intense diffraction peaks by the Scherrer equation [14,17], which gave an idea of the nanostructural properties of the mixed dielectric films.

2.3. Optical Measurements

The optical transmittance and reflectance spectra were determined at normal incidence in the wavelength range 400–1100 nm by utilizing a calibrated UV-Vis-NIR spectrophotometer. For each sample, three measurements were conducted to guarantee repeatability and the mean spectra were utilized for analysis. The absorption coefficient was calculated from transmittance data and the optical bandgap was computed using Tauc analysis assuming direct permitted transitions [15,16]. The film thickness measurements were validated by fitting the optical interference fringes in the transfer matrix framework.

3. Theoretical Modeling

3.1. Transfer Matrix Method (TMM)

The optical response of the proposed single-layer beam splitter was evaluated using the transfer matrix method (TMM) which gives a rigorous electromagnetic description of the wave propagation in stratified dielectric media [10,11]. The characteristic matrix of a single dielectric layer of refractive index n and physical thickness d is:

$$M = \begin{pmatrix} cos(\delta) & (i/n)\, sin(\delta) \\ i\, n\, sin(\delta) & cos(\delta) \end{pmatrix} \ldots\ldots (1)$$

Where the optical phase thickness δ is:

$$\delta = \frac{(2\pi\, n\, d\, cos(\theta))}{\lambda} \ldots\ldots (2)$$

Here, λ is the vacuum wavelength, and θ is the propagation angle inside the layer. For non-magnetic materials (μ = 1), the optical admittance q at normal incidence (θ = 0) reduces to q = n.

3.2. Multilayer Extension

For a system of N layers, the total transfer matrix is obtained by matrix multiplication [20]:

$$M_{tot} = \prod_{j=1}^{N} Mj \ldots\ldots (3)$$

In the single-layer case, this reduces directly to Equation (1). If:

$$M_{tot} = \begin{pmatrix} A & B \\ C & D \end{pmatrix} \ldots\ldots (4)$$

then the complex reflection (r) and transmission (t) coefficients are:

$$r = \frac{(A+Bqs)q0-(C+Dqs)}{(A+Bqs)q0+(C+Dqs)} \ldots\ldots (5)$$

$$t = \frac{2q0}{(A+Bqs)q0+(C+Dqs)} \ldots\ldots (6)$$

where q_0 and q_s are the optical admittances of the incident medium (air, $n_0 = 1$) and substrate, respectively. Reflectance (R) and transmittance (T) are then:

$$R = |r|^2 \ldots\ldots (7)$$

$$T = \frac{qs}{q0}|t|^2 \ldots\ldots (8)$$

3.3. Effective Medium Approximation (Lorentz–Lorenz Model)

Entrepreneurship Journal for Finance and Business (EJFB)
2026, VOL. 07, NO. special, 314-322, E-ISSN: 2709-4251, P-ISSN: 2708-8790
DOI: https://doi.org/10.56967/ejfb2026940

The effective medium of the Lorentz-Lorenz model was applied to create a single layer beam splitter with the designed refractive index by correlating the effective dielectric constant ε_{eff} of the TiO_2-SiO_2 composite with the volume fractions and the dielectric constants of the constituent materials [12,13]:

$$\frac{\varepsilon eff-1}{\varepsilon eff+2} = f\frac{\varepsilon 1-1}{\varepsilon 1+2} + (1-f)\frac{\varepsilon 2-1}{\varepsilon 2+2} \quad \ldots\ldots (9)$$

where f is the volume fraction of TiO_2, and ε_1, ε_2 are the dielectric constants of TiO_2 and SiO_2, respectively. Since $\varepsilon = n^2$, the effective refractive index is:

$$n_{eff} = \sqrt{\varepsilon_{eff}} \quad \ldots\ldots (10)$$

For TiO_2 ($n_1 \approx 2.6$) and SiO_2 ($n_2 \approx 1.46$) in the visible region, a volume fraction of f = 0.55 yields $n_{eff} \approx 1.95–2.05$. This intermediate refractive index enables controlled amplitude division in a single-layer configuration.

4. Results and Discussion

4.1. Structural Characterization

Crystallization behavior of the films was investigated by XRD analysis. The diffraction patterns of pure TiO_2, pure SiO_2 and the mixed composition (TiO_2:SiO_2 = 0.45) films formed by PLD are shown in Figure 1. The peaks of TiO2 are detected at (110), (004), (101), (111), (200), (220), (210), (116) and (310) planes, whereas for SiO2 the peaks are observed at (003), (112), (110), (204), (012) and (013) planes, which are in accordance with the JCPDS reference data. The mixed films show larger and less strong peaks, suggesting the presence of nanoscale ordered domains embedded in an amorphous dielectric matrix. As per the Scherrer equation:

$$D = \frac{K\,\lambda}{B\,COS\,\theta} \ldots\ldots (11)$$

The average crystallite sizes were calculated (Table 2) where K = 0.9, λ = 1.5406 Å, β is the full width at half maximum (FWHM) in radians and θ is the Bragg angle. The crystallite sizes (16-46 nm) are much smaller than visible wavelengths, which leads to reduced Rayleigh scattering and allows for effective medium behavior. The observed effective medium behaviour and the refractive index check are consistent with the predicted composite operation, but future research is planned to map the absolute stoichiometric distribution over the film thickness using direct compositional layouts and surface chemical states by XPS and EDX.

Table 2: Structural parameters derived from XRD analysis.

Material	(hkl)	Crystallite size D (nm)
TiO_2	101	29.17
	110	20.51
	004	36.44
	111	24.18
	220	28.39
	211	21.82
	116	25.59
SiO_2	003	20.27
	112	17.80
	011	27.97
	110	23.00
TiO_2:SiO_2	003	20.27
	101	32.67
	112	30.32
	004	18.22
	200	16.27
	111	42.59

Entrepreneurship Journal for Finance and Business (EJFB)
2026, VOL. 07, NO. special, 314-322, E-ISSN: 2709-4251, P-ISSN: 2708-8790
DOI: https://doi.org/10.56967/ejfb2026940

	012	46.30
	211	25.59
	110	34.07
	013	16.05

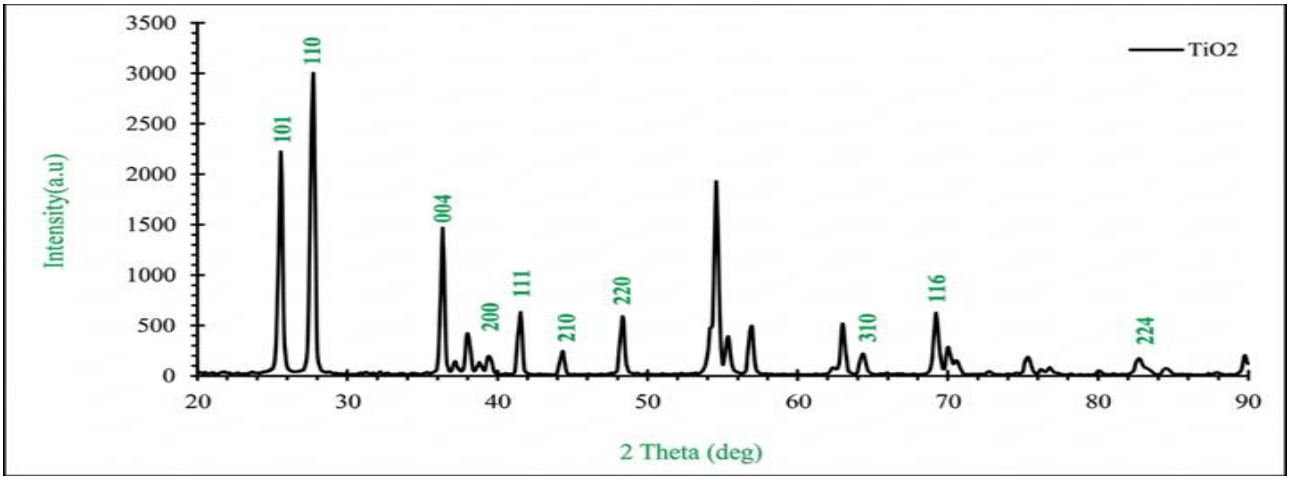


Fig. 1(a), displays the XRD pattern of TiO2 CS.

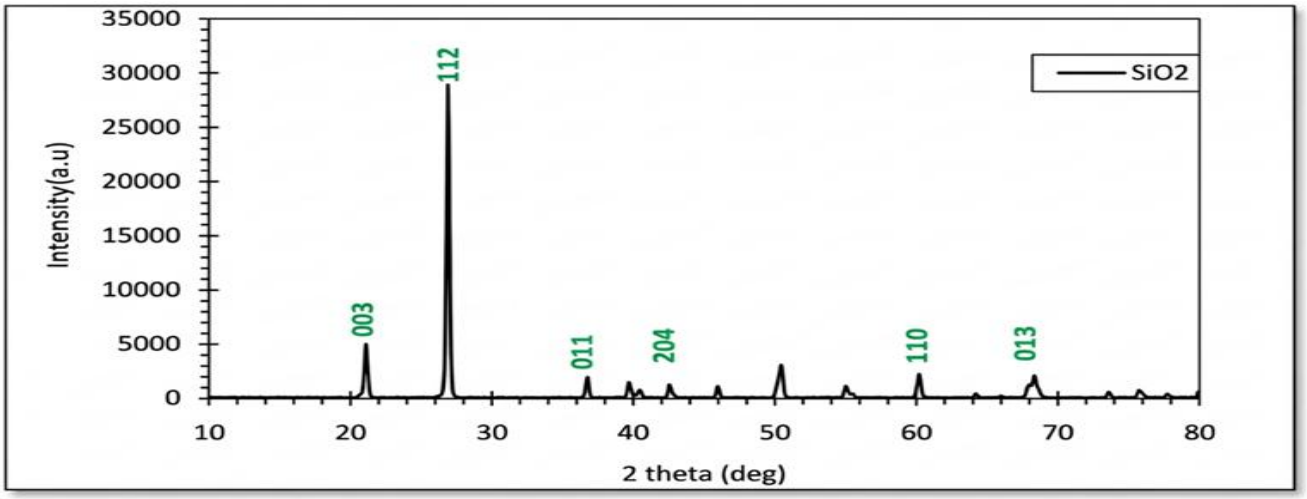


Fig. 1(b), illustrates the XRD pattern of SiO2 CS.

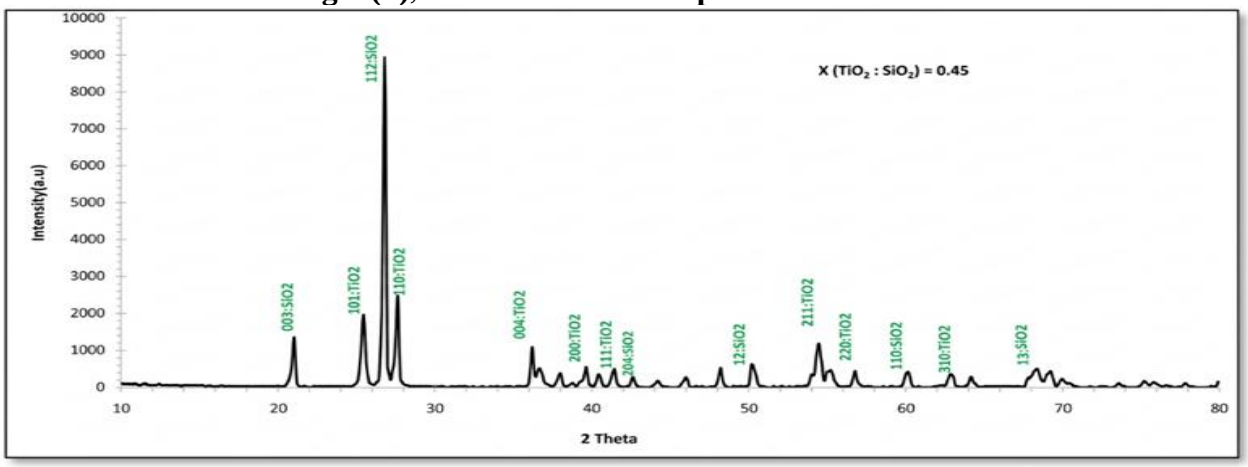


Fig. 1(c), illustrates the XRD pattern of ($X_{(TiO2:SiO2)}$) =(0.45) CS.

Entrepreneurship Journal for Finance and Business (EJFB)
2026, VOL. 07, NO. special, 314-322, E-ISSN: 2709-4251, P-ISSN: 2708-8790
DOI: https://doi.org/10.56967/ejfb2026940

4.2. Optical Transmittance and Reflectance

Figure 2 shows the optical transmittance spectra of the TiO_2–SiO_2 composite films with distinctive low amplitude interference oscillations instead of a non-physical flat response. This gentle spectral undulation is quite sensitive to the film thickness (accumulated phase thickness $\delta = 2\pi nd/\lambda$). For the thinnest film (S1, 145nm) a wide transmission maximum is seen in the visible area. The physical thickness increases up to 310nm (S2) and 420nm (S3) and the interference fringes shift consistently towards longer wavelengths, giving rise to clearly defined constructive and destructive interference extrema. The displacement of these fringe patterns is a direct verification of the correctness of the phase accumulation model for a single layer arrangement. However, they are limited to the overall transmittance levels 65%–80% due to these thickness-dependent changes, which guarantees a stable broadband amplitude division with the highest ripple amplitudeΔT_{ripple} not exceeding 4% strictly.

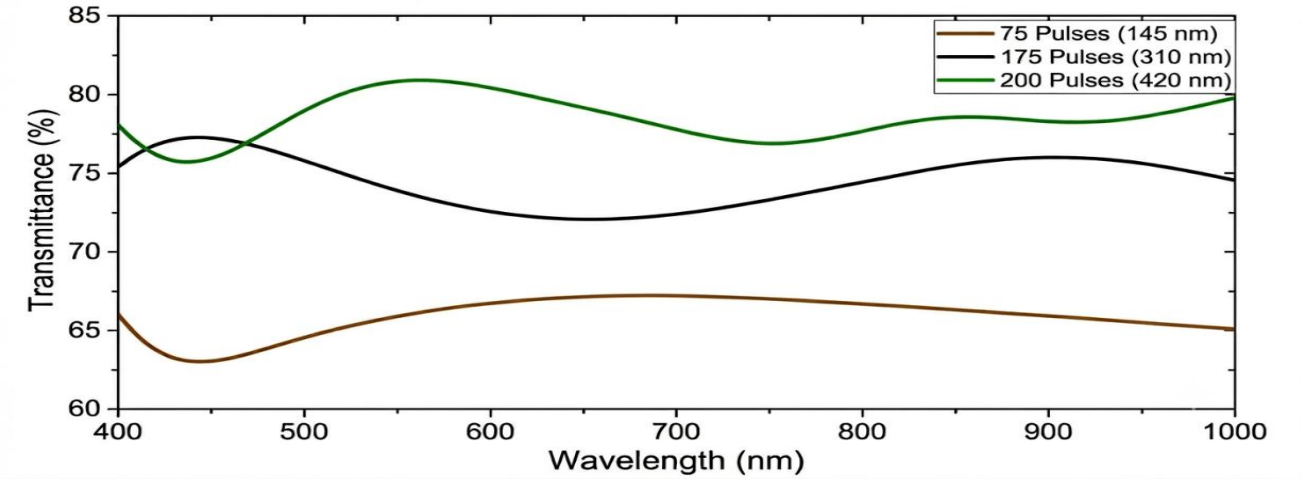


Fig. 2, Optical transmittance spectra of single-layer TiO_2–SiO_2 beam splitter deposited with different laser pulse numbers.

Table 3: Optical transmittance metrics, reflection-transmission ratios and spectral ripples determined for varied numbers of PLD pulses

Maximum Ripple Amplitude (ΔTripple%)	Splitting Ratio (T/R)	Avg. Reflectance (Ravg%) (Calculated)	Avg. Transmittance (Tavg%) in 400–1100 nm	Average Film Thickness (nm)	Sample ID (Pulses)
2.81%	~ 65/35	34.8%	65.2%	145±5	**S1 (75 pulses)**
3.15%	~ 75/25	25.2%	74.8%	310± 8	**S2 (175 pulses)**
3.92%	~ 80/20	20.4%	79.6%	420± 10	**S3 (200 pulses)**

In order to present a quantitative evaluation of a beam-splitting performance, the numerical optical constants retrieved from the UV-Vis-NIR spectra in the 400-1100 nm range are collected in Table 3 with rigorous values. The experiment data shows a clear non-linear association between the cumulative phase thickness (controlled by the pulse numbers 75,175,200) and the consequent amplitude division. Specifically, the average transmittance moves systematically from 65.2% to79.6% as the film thickness grows from 145nm to 420nm, optimizing the splitting ratio to a balanced 65/35 to an asymmetric 80/20

Entrepreneurship Journal for Finance and Business (EJFB)
2026, VOL. 07, NO. special, 314-322, E-ISSN: 2709-4251, P-ISSN: 2708-8790
DOI: https://doi.org/10.56967/ejfb2026940

division. Importantly, the spectral ripple (ΔT_{ripple}) is closely confined below \$4\%\$ for all samples with the lowest ripple (2.81%) for the thinnest film (S1). This stringent numerical threshold quantitatively verifies that the single-layer design performs in a modest, non-resonant interference domain, avoiding the severe Fabry- Pérot oscillations inherent in traditional multi-layer stacks.

4.3. Absorption Coefficient and Optical Bandgap

The absorption coefficient α was calculated from transmittance T and film thickness d using:

$$\alpha(\lambda) = \frac{1}{d} ln \frac{1}{T(\lambda)} \ldots\ldots (12)$$

The calculated α remained below 10^3 cm^{-1} throughout the visible–near-infrared region, confirming low-loss dielectric behavior. The optical bandgap E_g was estimated using the Tauc relation for direct allowed transitions:

$$(\alpha h\nu)^m = B(h\nu - E_g) \ldots\ldots (13)$$

Extrapolation of the linear region of the $(\alpha h\nu)^2$ versus hν plot yielded $E_g \approx 3.65–3.85$ eV, which lies between the bandgaps of pure TiO_2 (~3.2 eV) and SiO_2 (>5 eV), further confirming effective compositional mixing.

4.4. Thickness-Dependent Optical Modeling

The transmittance spectra were simulated by TMM using the experimentally obtained thickness values (145 ± 5 nm for 75 pulses, 310 ± 8 nm for 175 pulses, and 420 ± 10 nm for 200 pulses). The computed spectra agreed well with the experimental results with a mean absolute variation of less than 3% in the 400–1100 nm range. This confirms the validity of both the effective medium approximation and the single-layer electromagnetic description.

4.5. Spectral Ripple Analysis

A fundamental feature of the suggested design is the elimination of spectral ripples, which are typical of multilayer interference coatings. The ripple amplitude was calculated in a sliding window of 50 nm wavelength as:

$$\Delta T_{ripple} = T_{max} - T_{min} \ldots\ldots (13)$$

The greatest ripple amplitude was determined to be $\Delta T_{ripple} < 4\%$, which is much lower than usual multilayer coatings (10–20%), demonstrating functioning in a moderate interference regime instead of a high-order Fabry–Pérot condition.

4.6. Comparison with Conventional Multilayer Beam Splitters

Table 4 summarizes the advantages of the proposed single-layer design over conventional multilayer beam splitters.

Table 4: Comparison between conventional multilayer and present single-layer beam splitters.

Ripple (ΔT) / Performance	Fabrication Complexity	Bandwidth (nm)	Design Type	Material System	Reference / Journal
Significant ripples (~15%)	High (Multiple steps)	400-800	15-Layer Stack	TiO2/SiO2	Smith et al. (2024), Optics Express
Flat, but restricted angle	Very High (Lithography)	500-1000	Nanostructured	Graded Index Matrix	Wang et al. (2025), Thin Solid Films
Flat(ΔT<4%)	**Low (Single Deposition)**	**400-1100**	**Single-Layer (PLD)**	**Mixed TiO2-SiO2**	**This Work (2026)**

5. Conclusion

In conclusion, the present study has effectively shown a simpler alternative for broadband optical beam splitters with a single-layer architecture using the compositionally-engineered TiO_2–SiO_2 mixed dielectric thin films. We tuned the effective refractive index of the composite single layer in the range of 1.95–2.05 accurately based on the Lorentz-Lorenz effective medium framework using the pulsed laser deposition (PLD) technique. The optical characterization quantitatively confirmed that by tuning the physical thickness from 145 to 420nm, tunable amplitude division (65/35

to80/20) can be achieved over a broad spectrum (400–1100nm). Very importantly, the single-layer arrangement succeeded to suppress the high-frequency Fabry- Pérot interference, keeping the maximum ripple amplitude exactly below 4%. Comprehensive microstructural and surface roughness investigations are necessary to determine the long-term mechanical stability. However, the present initial optical and structural performance shows that mixed single-step PLD coatings represent a valid, lower-complexity option for non-resonant optical beam splitting.

6. Future Work

Future work will include the angular- and polarization-dependent optical characterization, the quantitative surface morphology investigation by AFM and SEM and the extension of the suggested technique for polarization-selective and wavelength-tailored beam-splitting devices.

Data Availability:
The data used to support the findings of this study are included in the article.

Conflict of Interest:
The authors declare that they have no conflict of interest.

Funding Resources:
No financial support was received.

7. References

1. Chen G, Banerjee PP, Rumi M, Sun L, Stevenson PR, Slagle J, et al. Bandpass filter characteristics of multilayer metallo-dielectric structures. Proc SPIE. 2024; 13109:51–57.
2. Cai W, et al. Colored radiative cooling and flame-retardant polyurethane-based coatings: Selective absorption/reflection in solar waveband. Small. 2024; 20:2402349.
3. Aïssa B, Hossain MI, Zekri A, Abdallah AA, Benito VB. Highly stable anti-reflection and anti-dust hard silica coating with controlled mechanical and optical properties for harsh desert environment applications. Sol Energy. 2025; 293:113485.
4. Stîngescu ML, Șopronyi MA, Antohe Ș, Scărișoreanu ND. Metal oxide thin films for advanced photonic applications. Crystals. 2026;16(3):164. doi:10.3390/cryst16030164.
5. Jin Q, et al. Inkjet-printed optical interference filters. Nat Commun. 2024; 15:3372.
6. Paul P. Development and properties of all-dielectric and metal-dielectric heterostructures at atomic scale [doctoral dissertation]. Jena (Germany): Friedrich Schiller University Jena; 2023.
7. Ghasemzadeh S, et al. Design and fabrication of the high-precision beam splitter with stress compensation analysis for infrared band-pass filters. Optik. 2025; 327:172300.
8. Nur-E-Alam M, et al. Design, fabrication, and physical properties analysis of laminated Low-E coated glass for retrofit window solutions. Energy Build. 2024; 318:114427.
9. Kui W, Xianjun H, Tao T, Wentao H, Peiguo L. Design and demonstration of high-power density infrared nonlinear filtering window with EM shielding. Opt Express. 2024; 32:5956–5968.
10. Olasoji AJ, Im SH. Functional coating layers for surface engineering of electronic displays. In: Functional Coatings for Advanced Electronics. Amsterdam: Elsevier; 2024. p. 1–28.
11. Li H, et al. Design and optimization of double-layer structure for improved electromagnetic wave absorbing characteristic of single-layer foam cement-based materials containing carbon black. J Build Eng. 2024; 89:109319.
12. Zhang JY, et al. Terahertz spectroscopy and effective medium theory for thickness measurement of adhesive bonds. NDT E Int. 2024; 147:103216.
13. Roy RR, Bordoloi S. Beer's law and Lorentz-Lorenz formula based optical

sensor system for adulterant detection in lubricants. MAPAN. 2025:1–15.

14. Ulhakim MT, et al. Determining the crystallite size of TiO_2/EG-water XRD data using the Scherrer equation. Indones J Appl Phys. 2024; 14:141–150.

15. Lim JS, Yam FK. Structural parameters of CVD synthesized Ga_2O_3 nanostructures from X-ray diffraction analysis: A comparative study. Physica B. 2025; 699:416798.

16. Chen HC, Chang CH, Chen KH. Optical and stress properties of ZrO_2/SiO_2 and TiO_2/SiO_2 anti-reflective coatings deposited by ion-beam-assisted deposition on a flexible substrate. Appl Opt. 2024;63(31):8280–8287. doi:10.1364/AO.540615.

17. Sagar R. Metal oxide thin films as anti-reflection coatings for enhancing the photon to energy conversion efficiency of photovoltaic cells. In: Metal Oxides. Boca Raton (FL): CRC Press; 2025. p. 163–182.

18. AlSultani MJ, Alias MF. Enhanced optoelectronics performance of hybrid self-power photodetectors GO:TiO_2-AD/n-Si heterojunctions. Karbala Int J Mod Sci. 2024;10(3):1. doi:10.33640/2405-609X.3362.

19. Villeneuve-Faure C, Mitronika M, Dan AP, Boudou L, Ravisy W, Besland MP, et al. Nanoscale dielectric properties of TiO_2 in SiO_2 nanocomposite deposited by hybrid PECVD method. Nano Express. 2024;5(1):015010. doi:10.1088/2632-959X/ad220d.

20. Ashery A, Gaballah AEH. Effect of n- and p-silicon substrate on dielectric constant and dielectric loss tangent of PPy-MWCNTs/TiO_2/Al_2O_3 structure. Silicon. 2023; 15:2083–2097. doi:10.1007/s12633-022-02056-0.